ORIGINAL ARTICLE

What makes a hydrogel-based dressing advantageous for the prevention of medical device-related pressure ulcers

Angela Grigatti | Amit Gefen [ORCID]

Department of Biomedical Engineering, Faculty of Engineering, Tel Aviv University, Tel Aviv, Israel

Correspondence
Amit Gefen, The Herbert J. Berman Chair in Vascular Bioengineering, Department of Biomedical Engineering, Faculty of Engineering, Tel Aviv University, Tel Aviv 6997801, Israel.
Email: gefen@tauex.tau.ac.il

Abstract

The synergistic influences of geometrical, mechanical and thermal mismatches between a skin-contacting medical device and the skin may cause tissue stress concentrations and sharp temperature gradients, both of which contribute to the risk for medical device-related pressure ulcers. In this work, we developed an innovative, integrated experimental bioengineering approach encompassing mechanical stiffness, friction and thermal property studies for testing the biomechanical suitability of a hydrogel-based dressing in prophylaxis of injuries caused by devices. We characterised the viscoelastic stress relaxation of the dressing and determined its long-term elastic modulus. We further measured the coefficient of friction of the hydrogel-based dressing at dressing-device and skin-dressing interfaces, using a tilting-table tribometer. Lastly, we measured the thermal conductivity of the dressing, using a heat-flow meter and infrared thermography-based method. All measurements considered dry and moist conditions, the latter simulating skin perspiration effects. Our results revealed that the long-term stiffness and the thermal conductivity of the hydrogel-based dressing matched the corresponding properties of human skin for both dry and moist conditions. The dressing further demonstrated a relatively high coefficient of friction at its skin-facing and device-facing aspects, indicating minimal frictional sliding. All these properties make the above dressing advantageous for prevention of device-related injuries.

KEYWORDS
friction properties, MDRPUs, pressure injury, thermal conductivity, wound care

Key Messages
- stiffness/thermal property matching is vital to protect skin from injury by devices
- prophylactic dressings must stay in place and should not frictionally slide on skin
- a hydrogel-based dressing was experimentally evaluated to address these points

- the tested dressing exhibited adequate mechanical and thermal performances
- hydrogel-based dressings are suitable for preventing device-related injuries

1 | INTRODUCTION

In the last years, it has become increasingly apparent that medical device-related pressure ulcers (MDRPUs) represent a significant burden to both patients and healthcare providers.[1,2] MDRPUs may be caused by skin-contacting devices, which are applied for either diagnostic or therapeutic purposes and are defined as "injuries which involve interaction with a device or object that is in direct or indirect contact with skin … causing focal and localised forces that deform the superficial and deep underlying tissues."[3] Common causes of MDRPUs are poor positioning of the applied device, use of ill-fitting devices (eg, to the size or age of the patient or to the treated body part) or otherwise, incorrect application of a device; the shape of the injury caused by the device generally conforms to the pattern or shape of the device itself.[4] Importantly, etiological works reported in the past few years demonstrated that MDRPUs are generated by the synergistic influences of geometrical, mechanical and thermal mismatches between a skin-contacting medical device and the skin (and underlying tissues). For example, a considerable mismatch between the device material stiffness (at the part of the device that comes into contact with skin) and the stiffness of native skin, which typically implies that the device materials are substantially stiffer (or are nearly rigid) with respect to skin, cause skin and underlying tissue stress concentrations.[1,5-12] Likewise, a mismatch in thermal properties between a device and tissues does not allow effective transfer of metabolic heat from the skin to the environment and thereby may lead to sharp temperature gradients that increase the metabolic demand of tissues and make them more susceptible to ischemic damage.[7,13] The recent work of an International Expert Panel have identified three specific bioengineering factors that are considered to play an important role in the development of MDRPUs[7]: (a) The generic designs of common skin-contacting medical devices, which do not accommodate to the variability in body sizes and shapes across patients (ie, a geometrical mismatch). (b) The device materials at and near the interfaces with skin, which are substantially stiffer than the skin and subdermal tissues (ie, a mechanical stiffness mismatch). (c) The microclimatic changes near the skin surface due to medical devices placed on the skin, which impedes conductive, convective and evaporative heat and

moisture loss from the skin[14] (ie, a thermal mismatch). The latter factor (indirectly) negatively impacts the mechanical and tribological properties of the skin region facing the medical device, which ultimately leads to more vulnerable skin and underlying tissues.

Continuous positive airway pressure (CPAP) masks are among the medical devices most commonly associated with MDRPUs, in both paediatric and adult patients and at acute care as well as post-acute and long-term care settings.[15,16] The use of ward based non-invasive ventilation employing CPAP masks is increasing sharply, with approximately 9000 reported episodes yearly within the United Kingdom prior to the COVID pandemic.[17] Clearly, with respiratory failure due to the coronavirus 2019 (COVID-19) pandemic, which broke out in 2020 and that accelerated the use of CPAP masks as a first-line treatment for low oxygen saturation, these numbers must have increased substantially since they were reported (in the aforementioned work) in 2019. A comprehensive literature review of 62 randomised clinical trials indicated that the incidence rate of skin damage associated with CPAP (mostly nasal lesions) is between 5% and 50%; however, this rate increased to nearly 100% after 48 hours on CPAP ventilation.[16] The deformation damage in soft tissues may be aggravated if the straps of the CPAP mask are overtightened; lesions were reported to develop as a result of the intense pressures exerted by the mask on facial skin, which can approach 70 mm Hg.[18] Development of a CPAP-related injury, typically on the bridge of the nose, chin or cheeks impacts both the efficacy of the intervention (or the ability to resume it) and the quality of life of the affected patient shortly after the injury but also in the long-term, due to potential permanent facial scarring, which may affect the body image.[19-24]

The prophylactic use of dressings or dressing cuts in the prevention of MDRPUs has been largely discussed in the literature, whereas the use of soft silicone[25] and polyurethane foam dressings,[26] silicone gel sheets,[26] and especially hydrocolloid dressings[27] is reported, showing that 40% to 75% of the MDRPUs occurrence can be avoided using dressings for prophylaxis.[3,28] Even though the prophylactic use of dressings has been widely discussed, dressings differ considerably in their biomechanical performances for prophylactic applications depending on their materials, composition and structure and therefore, it is imperative to select a dressing that is appropriate to

the individual and the clinical use.[3,29,30] In the context of preventing MDRPUs, our research group extensively studied the biomechanical protective effects of different dressing types, as well as an alternative approach of using a cyanoacrylate skin protectant.[9,10,31-33] In particular, in the aforementioned works, we have characterised the mechanical properties and behaviours of dressing materials and structures; the coefficient of friction (COF) at the dressing-skin interface, including under the effect of skin moisture; and the thermal conductivity of dressings intended for prophylactic use. The latter thermal property, which is critically important for assessing the expected microclimate environment induced by dressings in prophylactic use, has been investigated by means of a custom-made heat-flow meter as well as by using infrared thermography (IRT).[10,13,31]

The above dressing properties are all interacting in prophylactic use, in affecting the skin health status. For example, an increased skin moisture at a certain body region compromises the integrity and mechanical strength of the superficial skin, which makes it less tolerant to sustained mechanical loading and in particular, to the stress concentrations induced by a contacting device[14,31,34] The stiffness of the material/object with respect to that of skin and the underlying tissues will impact the magnitudes and spread of the aforementioned tissue stress concentrations; the more rigid the material/object, the higher the stress peaks that are expected in skin and underlying tissues. The likelihood of skin breakdown as a result of these device-induced tissue stress concentrations will depend on the intensity and extent of diffusion of these mechanical stresses into the skin depth and beyond, which in turn depends on the moisture level and the hydration of skin. In addition, the localised skin temperature is an important biomechanical factor contributing to the corresponding skin moisture, since heat accumulation at the skin-device interface leads to locally elevated skin temperatures and hence, to potential changes in the skin microbiome, compromised skin barrier functions and eventually, to weakening of the stratum corneum and epidermis as well as to increased sweating.[31] Therefore, it is vital to determine the mechanical stiffness properties and extent of thermal insulation of any materials/objects that are applied on the skin of a patient, relative to the corresponding native skin properties.

Considering the above bioengineering concepts and principles, the objective of this study was to assess, for the first time in the literature, the suitability of a hydrogel-based dressing for prophylactic use, through rigorous experimental testing of the mechanical, frictional and thermal properties of this specific dressing type, in both dry and moist conditions (as clinically relevant). In particular, this work evaluated the extent by which hydrogel-based dressings, once applied on facial skin in preparation for non-invasive CPAP ventilation, can protect the skin in all three aspects of mechanical, frictional and thermal performances.

2 | METHODS

Bioengineering laboratory testing was conducted to determine the mechanical, frictional and thermal behaviours and properties of a hydrogel-based dressing (HydroTac Transparent, manufactured by Paul Hartmann AG, Heidenheim, Germany), for evaluating the biomechanical suitability of this hydrogel-based dressing in prophylaxis of MDRPUs,[31] as detailed below.

2.1 | Simulation of a moist environment

Dressings were assessed in both their dry ("straight from the package") and moist conditions, given that medical devices associated with MDRPUs such as CPAP masks and ventilation tubing often induce or are applied in a moist environment for the dressing and skin. For simulating such moist dressing conditions, an isotonic 0.9%-saline solution was first prepared, using 9 g of NaCl in 1 L of distilled water,[35] boiled for up to 15 minutes to let the solute dissolve completely. After allowing the saline solution to cool down to room temperature, it has been uniformly sprayed on a flat semipermeable surface of a 0.8 ± 0.1 mm-thick dense chamois clothe,[36] simulating a perspiring epidermis*.[37,38] A dressing was then placed on the moist clothe and under a flat 390 g weight, which simulated a contact force level applied by adult CPAP masks.[10] The dressing was kept between the weight and the moist clothe for 2 hours,[39] after hermetically covering the set-up to minimise evaporation. Considering that the maximum sweat rate for healthy adults is 1 mg/min per cm^2,[40] a uniform layer of 12 ml of saline solution was applied to the chamois cloth immediately before applying the weight and then again an hour later, which approximates the flow rate of the perspiration over the skin-contacting dressing surface. After the aforementioned 2 hours treatment, dressings were released from the weights and disks were cut from each dressing, to form test specimens with the proper dimensions to determine the mechanical, frictional and thermal properties of the dressings, as described further.

2.2 | Compressive mechanical behaviour and properties of the dressing material

We determined the compressive stiffness of the dry and moist hydrogel-based dressings, considering their

potential viscoelastic response (in both conditions), through characterisation of their short-term and long-term elastic moduli using uniaxial unconfined compression testing. The present mechanical tests were based on the ASTM International standard test methods for rubber properties in compression,[41] as follows. A load cell with a nominal range of 2 kN ± 0.5% accuracy, connected to an electromechanical material testing machine (Instron Corp., model 5944, Norwood, Massachusetts) operating with BlueHill software (Instron Corp. ver. 4.21, 2017), was used to apply the load via flat compression anvils, which were made larger than the dressing specimen surface area to ensure full contact. The size of the disk-shaped test specimens was standardised to a diameter of 28.6 ± 0.1 mm and thickness of 12.5 ± 0.5 mm. Each test specimen was obtained from a different (single) dressing and prepared immediately before the testing, to avoid any drying or evaporation effects and consequent changes of mechanical behaviour and properties. After measuring the thickness of each test specimen using a vernier calliper with a resolution of 0.05 mm, specimens were placed individually between the platens of the material testing machine. Thin sheets of sandpaper were further placed between the dressing specimen surfaces and the testing machine platens to avoid potential frictional sliding movements. Compressive forces were then applied at a displacement rate of 12 mm/min, up to a compressive strain of 50% (based on the undeformed measured thickness of the individual dressing specimen), after which the force was immediately released at the same (unloading) rate. This loading/unloading cycle was repeated a second time for preconditioning purposes, following which the force was similarly applied for a third time until a compressive strain of 50% was again reached, at which time the displacement was maintained so that the dressing remained compressed. The force data were measured instantaneously after the third ramp phase of the loading cycle and every 0.01 seconds thereafter, until changes in the measured force became less than 1%, which was considered as a plateau. After completion of the test, the force data were converted to stress using the individual specimen dimensions.[41] A stress-strain curve was then plotted for the third ramp phase of the loading cycle (per each trial), from which the instantaneous compressive elastic modulus (E_{ins}) was calculated, by linearizing the last 25% of the stress-strain curve. A stress-relaxation curve was further plotted from the "hold" phase of each trial, from which the long-term compressive elastic modulus (E_{lt}) was calculated, by averaging the last 25% of the stress-time curve. Measurements were repeated 10 times for dry and additional 10 times for moist dressing specimens.

2.3 | Frictional properties of the dressing material

We measured the static COF of the hydrogel-based dressing at its skin-dressing and dressing-device interfaces. For determining the COF at the latter interface, we used silicone pads with low and high surface roughness (HSR), to account for the wide range of manufacturer specifications for medical silicones that may be in contact with facial skin. Fresh porcine skin was used here as a substitute for human skin, due to its well-documented anatomical and physiological similarities to the human tissue and its widespread use in wound care research.[42,43] The porcine skin samples tested in these COF studies were obtained from 4-month-old female commercial pigs used for a different, unrelated (acute cardiovascular) study, which has been approved by the institutional review board of the Heart Institute of Sheba Medical Center (Ramat-Gan, Israel). The skin samples were extracted from the ventral area immediately after euthanasia and delivered fresh (on ice) to the laboratory for testing, which started approximately 30 minutes after harvesting the tissues. The skin samples were shaved-off before the testing and then cut into 18 × 10 cm rectangles.

All the present frictional measurements were conducted using a custom-made, electronically-controlled tilting-table tribometer with an effective testing area of 18 × 10 cm (Figure 1A), following an experimental protocol reported in our previously published work.[44] The static COF was evaluated for the following specific interfaces: (a) $f_{silicone-hydrogel}$, which is the static COF of the hydrogel-based dressings in their dry or moist conditions, against silicone with a HSR or with a low surface roughness (LSR); (b) $f_{hydrogel-skin}$ and $f_{hydrogel-Pskin}$, which are the static COFs of the hydrogel-based dressings in their dry and moist conditions, against fresh porcine skin with vs without simulated perspiration. A circular weight of 390 g with a diameter of 45 mm was applied in all test conditions to ensure full contact at the aforementioned interfaces and further, to simulate a sustained pressure from a medical device that occurs during the above frictional interactions, either on the outer surface of the hydrogel dressing or on the skin tissue samples directly.

The $f_{silicone-hydrogel}$ COF dataset was obtained by allowing a silicone layer characteristic to the materials used for padding the contours of CPAP masks to frictionally slide against the hydrogel-based dressings. Because the design of CPAP masks and in particular, the specification of the silicon pads, which are in contact with facial skin, varies across manufacturers, we have tested here two distinct silicone types that differ by their surface roughness. The difference in the surface roughness of the two tested

(A)

(B)
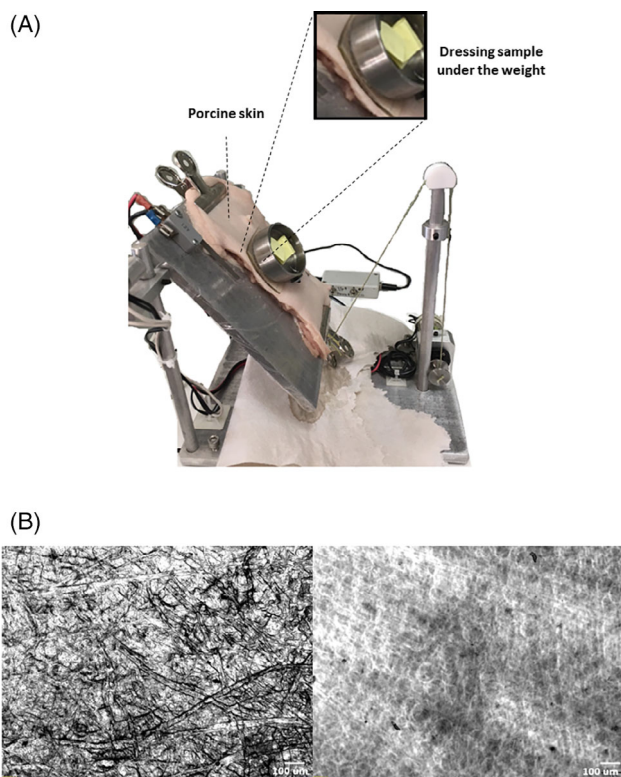
FIGURE 1   Measurements of the frictional properties at the dressing interfaces: A, The electronically-controlled tilting-table tribometer that has been developed in our laboratory for measurements of the coefficient of friction of materials used in the medical device industry against fresh skin tissue samples. A steel weight is applied on the dressing specimen tested against porcine skin to ensure uniform contact during the frictional sliding of the test specimen against the skin sample. B, Microscopy views of the high surface roughness (HSR, left frame) vs the low surface roughness (LSR, right frame) silicone sheets that represented medical device interfaces in this work. The difference in surface roughness was achieved by casting the silicone directly onto the Teflon surface of a mould in the LSR case vs onto a rough paper placed at the bottom of that mould in the HSR case

silicone pads has been achieved using two different substrata applied in preparing these silicone test samples. The HSR silicone was achieved by casting room-temperature-vulcanizing silicone onto a mould coated with rough paper, whereas the LSR silicone was made by casting the liquid silicone directly onto the Teflon surface of the mould. The HSR and LSR silicon pad surfaces were imaged using an optical inverted stereo microscope (Nikon Instruments Inc., model Eclipse TS100 obj. 4×, Tokyo, Japan) and photographed by means of a high-resolution digital camera (Olympus Corp., model EP50, Tokyo, Japan) (Figure 1B). A profilometer (KLA Corp., model Tencor P16, San Jose, California) was further used for quantitatively measuring the roughness difference between the HSR and LSR silicone sheets.

To measure the $f_{silicone-hydrogel}$ COF using the tribometer, a layer of either the HSR or LSR silicone was cut and glued to cover one flat aspect of the circular weight (Figure 1A). The aspect of the weight covered by the silicone layer was then allowed to frictionally slide against the external surface of the hydrogel-based dressing, which had been fixed to the tilting-table of the tribometer. Next, to determine the static COF at the silicone-dressing interface, the angle of the tilting-table was gradually and slowly increased by means of a computer-controlled electrical motor (Figure 1A) at a rate of 5°/min. As soon as the circular weight started to slide on the tilting-table of the tribometer due to the effect of gravity, an electrical switch opened, which instantaneously stopped the motion of the tilting-table at an angle ϑ, allowing to record the static COF as tan(ϑ).[44]

Similarly, to obtain the $f_{hydrogel-skin}$ COF data, the disk-shaped hydrogel dressing specimens were attached to the weight, so that their skin-facing side was allowed to frictionally slide against a specimen of fresh porcine skin that was attached to cover the entire effective test area of the tilting-table (Figure 1A). Lastly, $f_{hydrogel-Pskin}$ data were also collected. To mimic perspiration from the skin, 0.5 g of 0.9%-saline solution were uniformly sprayed onto the porcine skin prior to these measurements. This amount of saline solution was observed to induce a pearlescent effect (ie, the "pearls of sweat" that are characteristic to human skin perspiration). During these COF tests, the temperature and relative humidity were maintained at 25°C and 70%, respectively.

The hydrogel dressings were tested in both their dry and moist conditions, to form four different COF datasets: $f_{silicone-hydrogel}$ dry, $f_{silicone-hydrogel}$ moist, $f_{hydrogel-skin}$ dry and $f_{hydrogel-skin}$ moist (moistened dressings were obtained as described in Section 2.1 above). In addition to treating the dressings, a group of porcine skin specimens was sprayed with saline to simulate a perspiring skin, resulting in two additional COF datasets: $f_{hydrogel-Pskin}$ dry and $f_{hydrogel-Pskin}$ moist. Tests were repeated 10 times for each of these 6 COF test groups and per each silicone roughness level.

2.4 | Thermal conductivity of the dressing material

The thermal conductivity of the hydrogel-based dressing was measured using two different techniques, first by a heat-flow meter based on the cut-bar (axial heat flow) method[1] and second, through IRT according to the Bison and Grinzato protocol.[45]

2.4.1 | Heat-flow meter studies

The heat-flow meter testing device (Figure 2) contains two metal blocks, one made of aluminium and the other made of steel (each with a size of 4 × 4 × 5 cm), which are positioned above and below a slot for a dressing test specimen, respectively. Thermocouples, soldered along these metal blocks at symmetrically distanced locations relative to the dressing specimen slot, allow to acquire the temperature gradient across the block-specimen-block structure (Figure 2). Temperature readings from each of these thermocouples are digitally and automatically recorded into a computer using the LabVIEW data acquisition software (Version 19_f01, National Instruments, Austin, Texas). Two thermoelectric coolers (model TES1-12704 & TEC1-12715, Seeed Technology Co., Shenzen, China) controlled by an AC-DC multiple-switching 300 W power supplier (Model SH-300ATX, SkyHawk Telematics, St. John's, Newfoundland, Canada) function to warm the inferior
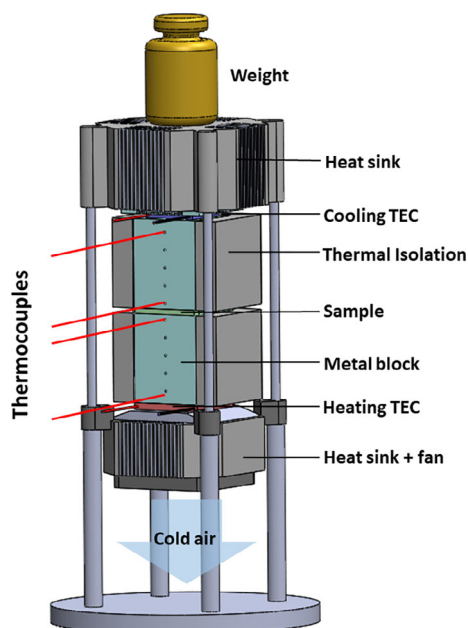
FIGURE 2 Schematic diagram of the heat-flow meter for thermal conductivity measurements of dressing materials. The dressing specimen is placed between hot and cold metal blocks. Four thermocouples are symmetrically distanced relative to the dressing sample slot (ie, two above and two below the dressing specimen) and allow to measure the thermal gradient across the dressing thickness. An external weight is placed on the top of the device, to simulate the pressure acting on the dressing specimen as it is placed between the skin and a medical device. The heat-flow meter is computer-controlled and temperature readings from all the thermocouples are automatically acquired and digitally stored for calculation of the thermal conductivity of the tested dressing material. The insulation that surrounds the system to facilitate a near-axial heat flow through the dressing thickness is not illustrated here for clarity of the internal construction of the heat-flow meter device. TEC, thermoelectric cooler

block and cool the superior block of the heat-flow meter (Figure 2). These two blocks were laterally insulated during the experiments using a 1-cm thick porous rubber sheet, which minimised the radial heat flow and therefore, imposed a nearly-unidirectional heat flux through the test device, perpendicularly to the dressing sample, so that the heat flux was transferred along the thickness axis of the dressing specimen. Consistent with the previously described (compressive stiffness and friction) studies, a 390 g weight has been applied on the superior surface of the heat-flow meter (Figure 2), which transferred pressure to the tested dressing specimen to impose full contact between the metal blocks and the dressing specimen and also simulate the sustained loading from a medical device.

Once the temperature readings from all the thermocouples have changed by less than 1% during a 10-minute time window, the system was considered to have reached a quasi-steady-state thermodynamic condition. The thermal conductivity coefficient k of the dressing material was then calculated, using the Fourier's law for a one-dimensional (1D) heat transfer process, under the assumption that the heat flux along the two metal blocks and the tested dressing in-between is equal, hence:

$$Q = k_{steel} \cdot A \cdot \frac{T_3 - T_{2B}}{X_{steel}} = k \cdot A \cdot \frac{T_{2B} - T_{2A}}{x}$$
$$= k_{aluminum} \cdot A \cdot \frac{T_{2A} - T_1}{X_{aluminum}} \quad (1)$$

where Q (W/m^2) is the axial heat flux, A (m^2) is the area of the tested dressing specimen in contact with the superior (cold) aluminium and inferior (warm) steel blocks of the heat-flow meter and T_{2A} (°C) and T_{2B} (°C) are the measured temperatures at the superior and inferior surfaces of the tested dressing specimen, respectively. The temperature T_1 (°C) is that of the highest thermocouple in the superior aluminium block, whereas T_3 (°C) is the temperature reading from the lowest thermocouple in the inferior steel block (Figure 2). The thicknesses of the dressing specimen, aluminium and steel blocks are x, $X_{aluminum}$ and X_{steel} (m), respectively. The (known) thermal conductivities of the (stainless, type 304) steel and aluminium blocks are $k_{steel} = 14.4$ W/mK and $k_{aluminum} = 240$ W/mK, respectively[46] (Equation (1)).

Reordering terms and isolating the parameter of interest, that is, the thermal conductivity of the dressing k (W/mK), yields:

$$k = \frac{k_{steel}}{X_{steel}} \cdot x \cdot \frac{T_3 - T_{2B}}{T_{2B} - T_{2A}} \quad (2)$$

The heat-flow meter was operated at ambient temperature and relative humidity of 25°C and 50%, respectively. Measurements were repeated 10 times for dry and additional 10 times for moist dressing specimens (the moisture conditions were induced as described in Section 2.1 above), thus resulting in two thermal conductivity datasets, of k_{dry} and k_{moist}, respectively (Equation (2)).

2.4.2 | IRT-based studies

An additional approach for thermal conductivity measurements, based on IRT imaging, was adopted from the work of Bison and Grinzato[45] for contactless evaluation of the thermal conductivity of the hydrogel-based dressings, to verify the previously described heat-flow meter studies. The IRT-based custom-made measurement system, which was used for these verification studies, is schematically shown in Figure 3A. The system consists of an aluminium heating panel (model MH-4, Fries Electric, Haifa, Israel) that directly heats the hydrogel-based dressing specimens, which have been piled up on this heating panel to form a bulk with lateral dimensions of 52×42 cm^2 and thickness of 1 cm. This bulk of five dressings piled up in a stack allows the IRT camera to have a larger object to focus on, which ultimately improves the accuracy of the thermal conductivity measurements. As with the previous method, a 390 g weight was placed on top of the dressing stack to simulate pressure from a medical device[10] and to ensure tight dressing-to-dressing and dressing-to-heating panel contacts (Figure 3A). Polystyrene plates with thickness of 5 cm that were cut-to-shape were attached tightly to three lateral aspects of the dressing stack, to form thermal insulation and minimise the adjacent air volume and circulation and therefore, potential heat losses due to radial conduction, convection or radiation from the tested dressing stack. One lateral aspect of the dressing stack was not insulated, to provide a field of view (FOV) for the IRT camera, which contained the thickness axis of the stack. Lastly, an insulating box with a 4×5 cm window that facilitated a line of sight for the IRT camera

FIGURE 3 The infrared thermography-based system for thermal conductivity measurements of dressing materials: A, A schematic diagram of the set-up. A dressing stack specimen is placed directly above a heating plate, with its three (lateral) sides tightly covered by thick polystyrene insulation. A weight on top of the dressing stack simulates the pressure from a medical device and further ensures tight contact of the dressing with the heating plate. Additional insulation is obtained using a box that completely surrounds the set-up (not shown). B, Thermal images are acquired using a 4×5 cm window made in the external insolation box for this purpose (from the aspect shown in the left frame). This example (right frame) shows the temperature gradient across a hydrogel-based dressing stack 30 minutes after the heating plate has reached a steady (50°C) temperature
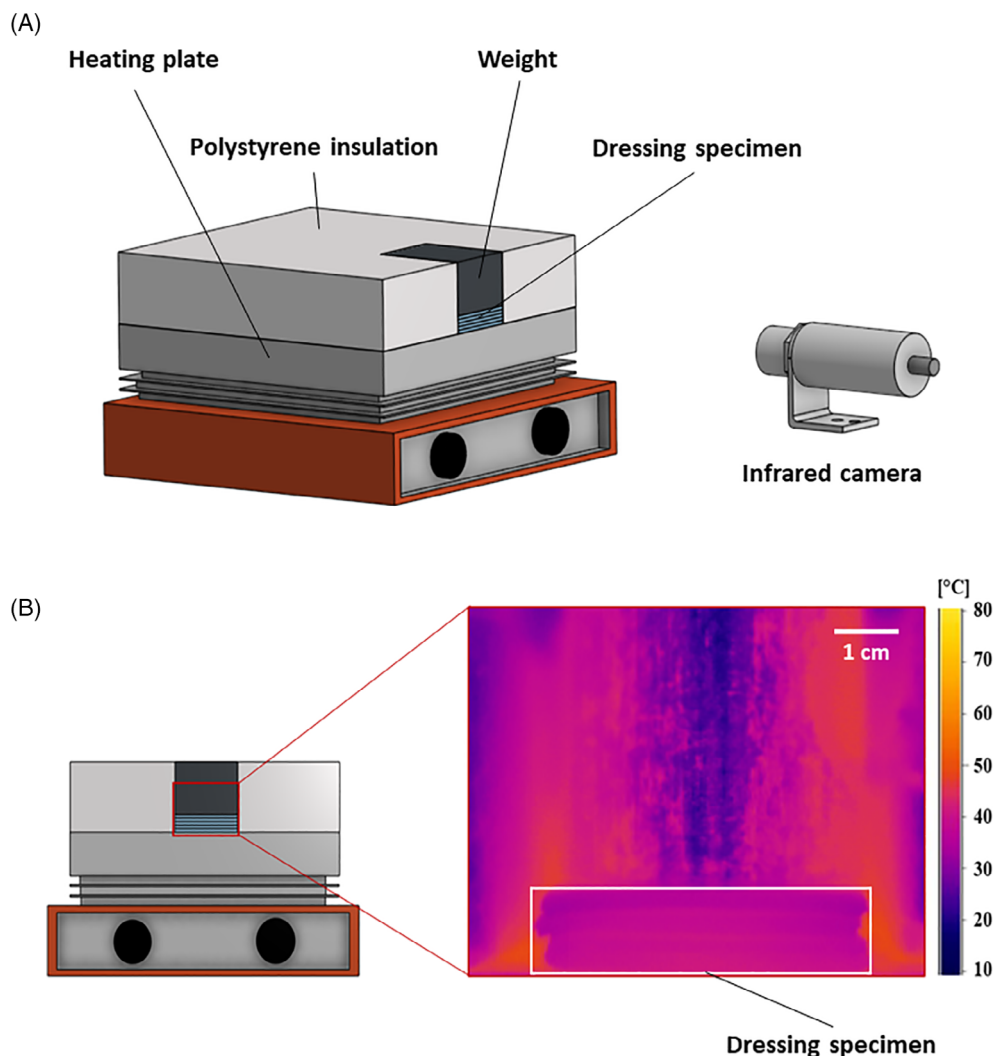
covered the entire measurement set-up, to further mini-mise potential heat exchange of the test specimen with the surroundings. The IRT camera (model Optris Xi 400, Optris GmbH, Berlin, Germany) was then placed and adjusted to measure the temperature gradient across the thickness axis of the dressing stack (Figure 3A). This IRT camera has a resolution of 382×288 pixels, an image frequency of 80 Hz, an object temperature range of 0°C to 250°C and an accuracy of ± 2°C. Three different values of emissivity have been selected to account for the different materials that were framed by the FOV of the IRT camera (Figure 3A): (a) $\epsilon_{aluminum} = 0.3$ for the heating plate; (b) $\epsilon_{water} = 0.98$ for the hydrogel-based dressings; and (c) $\epsilon_{steel} = 0.6$ for the applied precision weight.

Under the assumption of a uniaxial heat flow and steady-state thermal conditions, the thermal conductivity λ can be calculated using this IRT-based method, according to the first Fourier's law of heat conduction (Equation (3)):

$$\lambda = \frac{Q/A}{\Delta T/\Delta L} \quad (3)$$

where Q is the heat flux transferred through the cross-section A of the test specimen, thereby causing a temperature difference ΔT over a distance ΔL across the thickness axis of the specimen. According to the specific features of the present set-up (Figure 3A), Equation (3) can be rewritten as follows:

$$\lambda = \frac{Q_{heating\ plate}/A_{dressing\ specimen}}{\Delta T/\Delta L} \quad (4)$$

The term $\Delta T/\Delta L$ was evaluated as the resulting slope of the steady-state axial temperature profile measured using the IRT camera across the thickness of the dressing stack (Figure 3B). This slope term $\Delta T/\Delta L$, having units of (K/pixels) required a conversion factor of 5500 pixels/m to obtain λ in standard thermal conductivity units of (W/mK). Based on the thermal measurements by means of the heat-flow meter, as described in Section 2.4.1 above, a steady-state condition of the IRT measurement set-up was assumed to be reached 30 minutes after the heating plate was shown to maintain a steady temperature of 50°C. As in the previous testing method using the heat-flow meter, 10 dressing specimens were tested dry and additional 10 dressings were tested moist, resulting in λ_{dry} and λ_{moist} datasets, respectively.

2.5 | Data and statistical analyses

We first calculated descriptive statistics of means and SD for all the outcome measures listed above. A Grubb's (maximum normalised residual) test with $\alpha = 0.05$ was used to filter outlier data. For the compressive stiffness datasets (E_{ins} and E_{lt}, each at dry and moist dressing conditions), we conducted a two-way analysis of variance (ANOVA), followed by Tukey-Kramer post hoc pairwise comparisons, to identify potential statistically significant differences between the instantaneous and long-term compressive moduli and between the dry and moist testing conditions. For the COF datasets ($f_{silicone-hydrogel}$ dry, $f_{silicone-hydrogel}$ moist, $f_{hydrogel-skin}$ dry and $f_{hydrogel-skin}$ moist, $f_{hydrogel-Pskin}$ dry and $f_{hydrogel-Pskin}$ moist), we likewise ran ANOVA and Tukey-Kramer post hoc tests to determine whether the differences between the $f_{silicone-hydrogel}$ and

FIGURE 4 The stress (mean $\pm$ SD in grey shade) relaxation curves for dry (dashed line; n = 10) and moist (solid line; n = 10) hydrogel-based dressings. The instantaneous and near-instantaneous responses of the dressings that are irrelevant in the present context of medical device-related pressure ulcers (that take more than a few minutes to form) are not shown, to depict the details of the long-term responses

	E_{ins} (kPa)	E_{lt} (kPa)	Relaxation time[a] (min)	E_{ins}/E_{lt}
Dry dressings	495.7 ± 67.0	74.2 ± 15.9	2.63 ± 0.13	6.5 ± 0.6
Moist dressings	200.8 ± 27.4	21.0 ± 7.2	2.69 ± 0.08	10.5 ± 4.4

TABLE 1 The instantaneous (E_{ins}) and long-term (E_{lt}) compressive elastic moduli of the dry and moist hydrogel-based dressing specimens (mean $\pm$ SD)

Note: Tests were repeated 10 times for each condition.

[a]Relaxation time = the time at which the average stress data over a 10 seconds sampling window did not differ by more than 5% with respect to the stress data in a preceding, similar time window.

$f_{hydrogel-skin}$ COF data and between the dry and moist testing conditions were statistically significant. For the thermal conductivity datasets (which were obtained using two different test methods, that is, the heat-flow meter and IRT), we used separate unpaired, two-tailed t tests to determine whether the k_{dry} and k_{moist} and separately, the λ_{dry} and λ_{moist} were statistically distinguishable. This was followed by Bland-Altman (mean-difference) analyses, to evaluate the agreement between the k_{dry} and λ_{dry} datasets and separately, between the k_{moist} and λ_{moist} datasets. The level of statistical significance was set as $P < .05$ for all the above tests.

3 | RESULTS

3.1 | Compressive behaviour and properties

The compressive stress-relaxation curves of the hydrogel-based dressing materials, acquired at the dry and moist test conditions, are shown in Figure 4. The relevant descriptive statistics for the instantaneous (E_{ins}) and long-term (E_{lt}) compressive elastic moduli of the tested dressings and the relaxation times are provided in Table 1. Noteworthy is that after approximately 3 minutes, the stress-relaxation curves plateaued for both the dry and moist test conditions (Figure 4). The dressing materials further exhibited highly viscoelastic behaviour at both the dry and moist conditions, as the E_{ins}/E_{lt} ratios were substantially greater than unity at either condition (Table 1). It is further shown that the dry dressings were considerably stiffer than the moist ones, by ☐2.5-fold and ☐3.5-fold for E_{ins} and E_{lt}, respectively.

3.2 | Frictional properties

The profilometric characterisation of the silicone sheets used for the COF testing indicated peak-to-valley distances of approximately 41 and 11 μm for the HSR (Figure 1B; left frame) and LSR (Figure 1B; right frame) silicone specimens, respectively (Figure 5A). The mean surface roughness was statistically significantly ~4-times greater for the HSR silicone with respect to that of the LSR specimens (Figure 5B; $P < .05$). The ANOVA for the $f_{silicone-hydrogel}$ COF resulted in that moist dressing conditions did not significantly affect the COF for a given silicone roughness (Table 2). However, the LSR COFs were ~6.4-fold and ~7.1-fold significantly greater than the HSR COFs ($P < .01$) for the dry and moist dressing conditions, respectively, indicating greater frictional contact surface of the hydrogel-based dressing with the smoother silicone
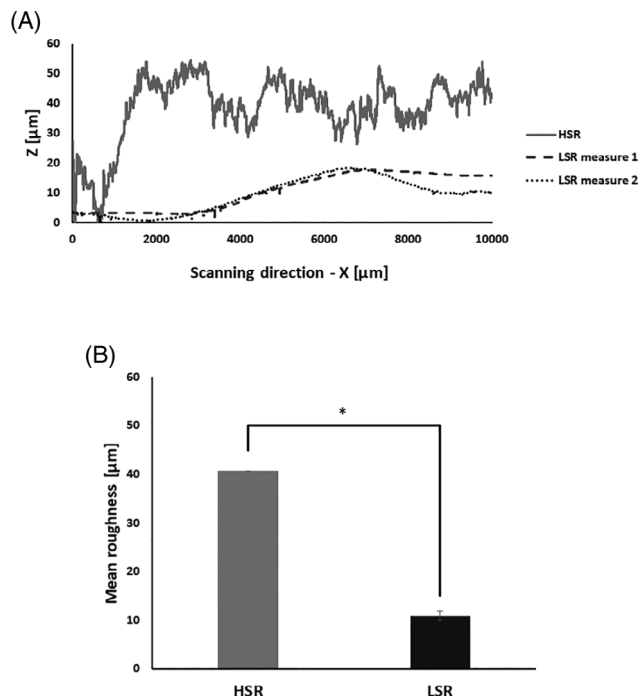
FIGURE 5 The surface roughness of the silicone sheets that simulated the medical device materials in contact with the tested dressings: A, The planar surface (peak-to-valley) topography of the high surface roughness (HSR) vs the low surface roughness (LSR) silicones along a 1-cm path of scanning. B, The average roughness (mean ± SD) for the HSR and LSR silicones (*$P \ll .01$)

TABLE 2 The coefficients of friction $f_{silicone-hydrogel}$ (means ± SD) of the hydrogel-based dressings in the dry and moist test conditions against silicone with high surface roughness (HSR) vs silicone with low surface roughness (LSR)

	Dry dressings		Moist dressings	
	HSR silicone	LSR silicone	HSR silicone	LSR silicone
$f_{silicone-hydrogel}$	0.77 ± 0.10	4.92 ± 2.13	0.76 ± 0.15	5.40 ± 2.39

Note: Tests were repeated 10 times for each condition.

TABLE 3 The coefficients of friction $f_{hydrogel-skin}$ and $f_{hydrogel-Pskin}$ (means ± SD) of the hydrogel-based dressings in the dry and moist test conditions against fresh porcine skin with vs without simulated perspiration

		Dry dressings	Moist dressings
No perspiration	($f_{hydrogel-skin}$)	1.38 ± 0	1.28 ± 0.04
Perspiration	($f_{hydrogel-Pskin}$)	1.38 ± 0.10	0.42 ± 0.02

Note: Tests were repeated 10 times for each condition.

TABLE 4 Thermal conductivity values (means $\pm$ SD) of the hydrogel-based dressings in the dry and moist test conditions measured using the heat-flow meter (k_{dry}, k_{moist}) and the infrared thermography-based method $(\lambda_{dry}, \lambda_{moist})$

Dry dressings		Moist dressings	
k_{dry}[a] (W/mK)	λ_{dry}[b] (W/mK)	k_{moist}[a] (W/mK)	λ_{moist}[b] (W/mK)
0.40 ± 0.02	0.31 ± 0.04	0.40 ± 0.03	0.36 ± 0.05

Note: Tests were repeated 10 times for each condition.

[a]The k_{dry}, k_{moist} values are statistically indistinguishable.

[b]The $\lambda_{dry}, \lambda_{moist}$ values are statistically indistinguishable after removing one outlier from the dry dressing dataset and one additional outlier from the moist dressing dataset.
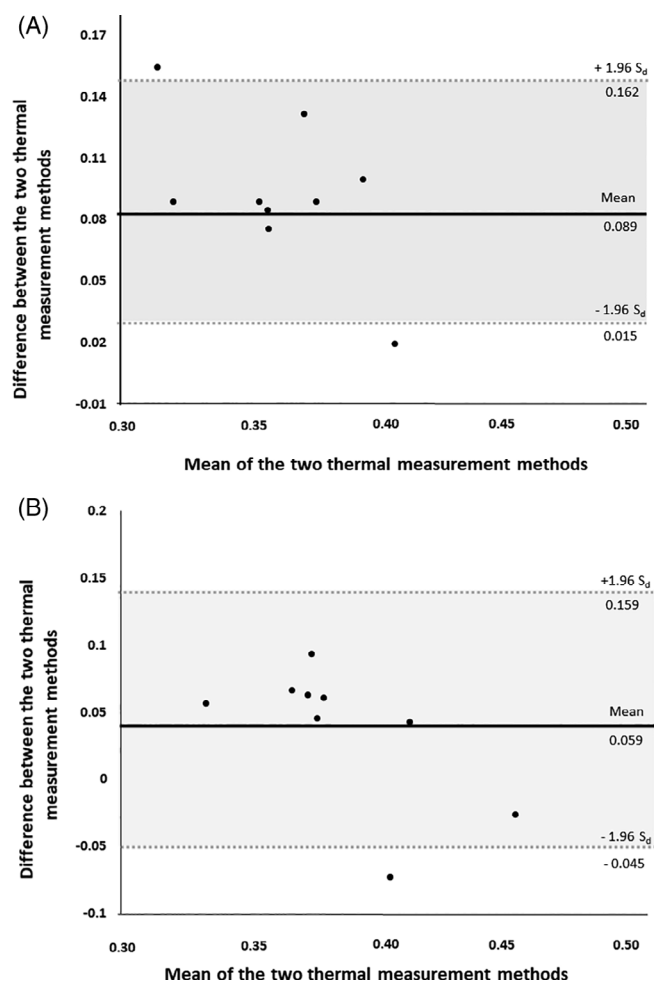
FIGURE 6 Bland-Altman (mean-difference) plots for the thermal conductivity values of the hydrogel-based dressings in their (A) dry and (B) moist conditions, as measured by the heat-flow meter vs the infrared thermography-based methods

surface (Table 2). In addition, the $f_{hydrogel-skin}$ and $f_{hydrogel-Pskin}$ COFs were indistinguishable for the dry dressing test condition, that is, the skin-dressing COF was unaffected by the simulated skin perspiration as long as the dressing did not become moist due to the contacting perspired skin (Table 3). Dressings, which were treated to become moist but that were then applied onto dry skin, exhibited

a relatively mild, yet statistically significantly ~7% decrease in their skin-dressing COF (Table 3; $P \ll .01$). Only moist dressings applied onto a simulated sweating skin demonstrated a more considerable, statistically significant ~70% reduction of the skin-dressing COF with respect to the dry dressing and dry skin test conditions (Table 3; $P \ll .01$).

3.3 | Thermal conductivity

The thermal conductivity coefficient of the dressings under investigation was not influenced by the moist test conditions, as shown by both the heat-flow meter and IRT-based methods (Table 4). Given the aforementioned statistical similarity between the dry and moist test conditions, thermal conductivity data were pooled per method type. Bland-Altman plots, comparing the outcome measures obtained using the two methods demonstrated that all but one data point were within the 95% limits of agreement, thereby justifying further pooling of the thermal conductivity values acquired by the heat-flow meter and IRT-based methods, to ultimately result in a mean thermal conductivity coefficient value of 0.37 ± 0.04 W/mK for the tested dressings (Figure 6).

4 | DISCUSSION

In this work, we developed and utilised an integrated experimental approach, encompassing mechanical stiffness, friction and thermal property studies to test the suitability of a hydrogel-based dressing for the prevention of MDRPUs. Etiological work reported in the past few years demonstrated that the synergistic influences of geometrical, mechanical and thermal mismatches between a skin-contacting medical device and the skin (and underlying tissues) of a patient cause tissue stress concentrations and sharp temperature gradients, which contribute to the MDRPU risk.[1,2,5-12,47,48] Ideally, the materials of a device, which are in continuous contact with skin, should have similar mechanical and thermal properties to those

of the native skin, to minimise the occurrence of mechanical stress and temperature gradients between the device and the skin and subdermal tissues. That is, there should be stiffness-matching and thermal conductivity-matching between the device materials and the adjacent tissues to the best possible extent.[7] Improving the design of basic and common medical devices such as CPAP masks, endotracheal tubes, cervical collars and other devices that are epidemiologically associated with high occurrences of MDRPUs,[7] driven by the above scientific findings, is a slow, cumbersome process that may take many years to complete, as these devices kept their traditional designs for decades. For example, endotracheal tubes are used for anaesthesia and ventilation since the second half of the 19th century and their fundamental design barely changed[48] and likewise, CPAP treatments invented by the Australian physician Professor Colin Sullivan in the early 1980s[49] did not evolve significantly since their introduction. With the present COVID-19 pandemic, which had massively accelerated the use of CPAP as a first-line treatment for low oxygen saturation, healthcare professionals needed solutions here and now, and so it became a common clinical practice to apply cuts of various dressing types to protect the skin under devices, including CPAP masks.[8] Different dressing materials have been clinically employed for the above purpose, mostly hydrocolloids[17,50] and under the circumstances of the pandemic, their use have been extended in the last year to also protect the skin of healthcare workers from personal protective equipment.[51] Nevertheless, while other dressing technologies may be equivalent or superior to the market-dominant hydrocolloids in protecting the skin under devices, no published knowledge exists on the suitability of hydrogel-based dressings for MDRPU prevention. Given the widespread use of non-invasive CPAP ventilation during the pandemic (following the discovery that it avoids intubation in one of two patients presented with an acute respiratory distress syndrome[52]) and the projected use of this particular device going forward, we have decided to focus here on interactions of hydrogel-based dressings with CPAP masks in a preventative context.

To consider the range of real-world mechanical and thermal conditions that are relevant to prophylactic use of the presently investigated hydrogel-based dressings under a CPAP device, the effects of moisture on the skin and dressing must be taken into account, as CPAP masks induce a highly moist and humid environment. The intra-mask relative humidity typically exceeds 80%,[53] which has been associated with excessive skin hydration and therefore increased skin fragility.[19] As the stress relaxation response of the tested hydrogel-based dressing material plateaued after approximately 3 minutes

already, under both the dry and moist test conditions, the long-term stiffness properties are the relevant ones in the context of MDRPUs, as a clinically significant injury is expected to develop after a substantially longer time, when the stiffness of the hydrogel has already stabilised (specific incidence rates of CPAP-related MDRPUs range from 5% to 50% for 2 to 4 hours of continuous CPAP usage and up to 100% after 48 hours of usage[16]). Hence, the long-term stiffness E_{lt} values of the hydrogel-based dressing, which were ~74 kPa and ~21 kPa for its dry and moist conditions, respectively (Table 1), should be assessed against the stiffness of living facial skin in a clinically relevant loading mode. The literature reports that the in vivo elastic moduli of facial skin, measured through indentation (which is the closest loading mode to the real-world skin-CPAP interaction) range from 5 to 180 kPa.[54-57] Hence, the stiffness of the tested hydrogel-based dressing falls within the low to mid-range of the reported skin stiffness data, which meet the stiffness-matching goal.

We further measured the static COFs at the dressing-device and skin-dressing interfaces using an electronically-controlled tilting-table system. Although we have considered two distinct silicone roughness levels for representing the CPAP pad, we surmise that the majority of the medical-grade silicones should have a LSR (for maintaining a tight seal to the face), hence the associated LSR COFs for the dressing-device interface are the more clinically relevant values. These COFs were approximately 5 (Table 2), which is considered high in the field of tribology and indicates a tacky response of the hydrogel-based dressing with the smooth silicone, also suggesting a good seal at that interface as required for effective CPAP treatments. Our data further revealed relatively high COFs for the skin-dressing interface, of ~1.3 to 1.4, as long as the skin was not moist (Table 3). Simulated perspiration of the skin reduced the latter COF to ~0.4 (Table 3), which is still up to 4-fold greater than the range of COFs reported for hydrogels in contact with artificial materials such as glass.[58] These findings altogether indicate that there should be negligible relative motion between an applied hydrogel-based dressing and a CPAP mask, or between the dressing and skin, unless both the dressing and skin become excessively moist. Thus, as long as the dressing and skin remain (relatively) dry, our results suggest that there will be minimal frictional deformations of skin and underlying tissues due to the tacky nature of this hydrogel-based dressing. Moreover, once applied onto dry skin, a new (out of package) hydrogel-based dressing is likely to gradually absorb perspiration until the dressing itself becomes nearly saturated, which implies that the moist dressing plus perspired skin conditions listed in Table 3 represent an extreme state in a

clinically relevant scenario, where the prophylactic dressings under the CPAP mask have not been replaced for a long time.

Lastly, the thermal conductivity of the hydrogel-based dressing was investigated and found to be 0.37 W/mK, which was unaffected by moisture. This finding, which is consistent with the literature[59,60] for polyacrylamide hydrogels and polymer gels is ~62% the thermal conductivity of pure water (~0.6 W/mK)[61,62] and importantly, falls within the mid-range of the thermal conductivities reported for human skin, which are 0.35 to 0.43 W/mK.[63,64] The recent work of Crawford and colleagues, which reported anatomical-site-specific skin thermal conductivity data, revealed that the thermal conductivity of skin at the nose (the skin at the bridge of the nose commonly breaks down under prolonged pressure by CPAP masks[19,53];) is 0.34 to 0.45 W/mK and that at the cheeks (which are also susceptible to injury by CPAP masks) is 0.39 to 0.45 W/mK.[65,66] The latter data indicate that the thermal conductivity of the hydrogel-based dressings studied here are similar to the thermal conductivity of facial skin at sites susceptible to MDRPUs with a maximum potential deviation of 18%, which is low in biological variability terms. Accordingly, as with stiffness, the presently investigated hydrogel-based dressings demonstrate optimal thermal conductivity-matching with human skin, which is not surprising given the ~60% to 80%-weight bound water contents in hydrogels,[67,68] which is similar to the water content in facial skin (that has a relatively high water content with respect to other skin sites: ~60% to 80%).[69-72]

Translation of bench science work concerning performance testing for dressings in prophylactic use into standard clinical practice requires development of new international testing standards and performance metrics, which will ultimately become a global benchmark for industry developers, regulators and healthcare professionals. Testing standards and corresponding manufacturing practices are established for all types of medical devices and may serve different stakeholders in various forms, such as by defining targets for industry research and development purposes or for formulating instructions for use. Regulatory bodies and reimbursement policymakers may use testing standards to evaluate the safety and efficacy of prototypes or existing products and to qualify products for use with specific patient groups. Importantly, the performance metrics that are provided by testing standards support informed clinical decision-making, by objectively identifying and quantitatively describing the strengths and weaknesses of technologies and products, which then facilitates systematic comparisons of product performances. Development work of such testing standards is now co-led by the senior author and is underway, in the framework of the prophylactic dressing standards initiative (https://www.epuap.org/prophylactic-dressing) of the US National Pressure Injury Advisory Panel and the European Pressure Ulcer Advisory Panel.

To conclude, the importance of mechanical stiffness-matching and thermal conductivity-matching between the part of a medical device, which is in prolonged contact with skin and the skin and underlying tissues adjacent to the applied device, has been highlighted in the up-to-date literature.[1,2,5,47] In particular, the literature concerning the aetiology of MDRPUs indicates that stiff polymeric materials in contact with skin may result in non-uniform pressure and shear distributions and elevated stresses on the interfacing skin and within underlying tissues.[1,6,10] These contact-related phenomena intensify in highly curved anatomical regions where the depth of soft tissues over the underlying bone is relatively small, the bridge of the nose being an extreme exemplifying case for these conditions.[1] Only by matching the mechanical stiffness properties of the applied device materials to those of skin and subdermal tissues and thereby guaranteeing a uniform mechanical load redistribution at and near the skin-device interface, tissue stress concentrations can be avoided and MDRPUs formation prevented. Nevertheless, re-designing common medical devices applied to skin such as CPAP masks is a long, expensive and laborious process with numerous regulatory and cost implications, which does not appear to be practical, especially at the COVID pandemic times where immediate solutions are needed. This is why dressings have been applied in clinical practice, as skin protectants under medical devices at relevant skin-device interfaces, but it is the role of bioengineers to guide medical teams in how to achieve optimal skin and underlying tissue protection by doing so, since not all dressings will perform equally. The present work takes a first step in establishing the bioengineering criteria, laboratory bench test protocols and performance metrics to determine and evaluate the device-dressing mechanical stiffness-matching.

Likewise, thermal mismatching between the device and underlying skin and subdermal tissues should be minimised and can be optimised through prophylactic use of dressings, to prevent MDRPUs by allowing effective release of metabolic heat from the skin to the environment.[7,13] A localised rise in skin temperature increases the metabolic tissue demand for cellular oxygen and nutrients, by approximately 10% per 1°C of skin temperature elevation. As a result, the blood perfusion increases locally, to minimise the accumulation of tissue waste, thereby reducing the tissue tolerance to ischemia and making it more susceptible to MDRPUs at lower interface pressure and shear levels.[31,73] A dressing used

for prophylaxis of MDRPUs should therefore have a thermal conductivity value that is close to that of living human skin, as to not create an insulating layer above the skin that would prevent effective heat release away from the skin to the environment.[13] Such dressing thermal conductivity, which matches that of native skin, would further facilitate uniform spread of any accumulated metabolic heat under the skin-facing aspect of the dressing, which again promotes effective heat transfer and reduces the likelihood that "hot spots" of elevated temperature would form on the skin under the dressing and subdermally.[6,13]

For all the above reasons, it is imperative that dressings used in prophylaxis of MDRPUs smooth the tissue load gradients—both thermal and mechanical—by matching (or bridging between) the device and tissue stiffness and thermal properties, so that with the effect of the dressings, the medical device elements contacting the skin (with the applied dressing) become at stiffness and thermal conductivity levels that are near those of the skin and underlying soft tissues.[7] In addition to that, frictional sliding between the applied device and the skin, resulting in skin distortions in shear, should be minimised.[7] Therefore, based on the compressive, frictional and thermal properties measured in this work, the hydrogel-based dressing under investigation has been shown to meet the primary requirements from a potent material for prevention of MDRPUs. Namely, the tested dressings exhibited stiffness-matching with skin, tacky ("stay in place") behaviour, which minimises frictional skin-device sliding and also skin-matching thermal conductivity that allows heat potentially accumulated in skin under the applied device to be transferred (through the dressing) onto the environment. Taken together, these mechanical and thermal properties make the presently tested hydrogel-based dressing advantageous for prevention of MDRPUs from a bioengineering perspective.

ACKNOWLEDGEMENTS

DATA AVAILABILITY STATEMENT

The data that support the findings of this study are available from the corresponding author upon reasonable request.

ORCID

Amit Gefen https://orcid.org/0000-0002-0223-7218

ENDNOTE

* Saline solution was chosen as the sweat substitute here, due to its osmolarity and composition, which contains common electrolytes (Na^+, Cl^+) that are characteristic to perspiration and/or humidity in a continuous positive airway pressure (CPAP) mask environment.

REFERENCES

1. Bader DL, Worsley PR, Gefen A. Bioengineering considerations in the prevention of medical device-related pressure ulcers. *Clin Biomech*. 2019;67:70-77. https://doi.org/10.1016/j.clinbiomech.2019.04.018.

2. Grigatti A, Gefen A. Pediatric medical device-related pressure injuries. In: Ciprandi G, ed. *Neonatal and Pediatric Wound Care*. Torino, Italy: Minerva Medica; 2021.

3. EPUAP/NPIAP/PPPIA (European Pressure Ulcer Advisory Panel, National Pressure Injury Advisory Panel and Pan Pacific Pressure Injury Alliance). In: Emily H. (ed). *Prevention and Treatment of Pressure Ulcers/Injuries: Quick Reference Guide*. 3rd ed. Westford, MA: EPUAP/NPIAP/PPPIA; 2019.

4. Black J, Alves P, Brindle CT, et al. Use of wound dressings to enhance prevention of pressure ulcers caused by medical devices. *Int Wound J*. 2015;12(3):322-327. https://doi.org/10.1111/iwj.12111.

5. Verberne JWR, Worsley PR, Bader DL. A 3D registration methodology to evaluate the goodness of fit at the individual-respiratory mask interface. *Comput Methods Biomech Biomed Engin*. 2020;1-12. https://doi.org/10.1080/10255842.2020.1849156.

6. Amrani G, Peko L, Hoffer O, Ovadia-Blechman Z, Gefen A. The microclimate under dressings applied to intact weight-bearing skin: infrared thermography studies. *Clin Biomech*. 2020;75:104994. https://doi.org/10.1016/j.clinbiomech.2020.104994.

7. Gefen A, Alves P, Ciprandi G, et al. Device-related pressure ulcers: SECURE prevention. *J Wound Care*. 2020;29(Sup2b):S1-S52. https://doi.org/10.12968/jowc.2020.29.Sup2a.S1.

8. Gefen A, Ousey K. Update to device-related pressure ulcers: SECURE prevention. COVID-19, face masks and skin damage. *J Wound Care*. 2020;29(5):245-259. https://doi.org/10.12968/jowc.2020.29.5.245.

9. Gefen A. The bioengineering theory of the key modes of action of a cyanoacrylate liquid skin protectant. *Int Wound J*. 2020;17(5):1396-1404. https://doi.org/10.1111/iwj.13401.

10. Peko Cohen L, Ovadia-Blechman Z, Hoffer O, Gefen A. Dressings cut to shape alleviate facial tissue loads while using an oxygen mask. *Int Wound J*. 2019;16(3):813-826. https://doi.org/10.1111/iwj.13101.

11. Lustig A, Margi R, Orlov A, Orlova D, Azaria L, Gefen A. The mechanobiology theory of the development of medical device-related pressure ulcers revealed through a cell-scale computational modeling framework. *Biomech Model Mechanobiol*. 2021;20:851-860. https://doi.org/10.1007/s10237-021-01432-w.

12. Levy A, Fader M, Bader D, Gefen A. Penile compression clamps: a model of the internal mechanical state of penile soft

tissues. *NeurourolUrodyn*. 2017;36(6):1645-1650. https://doi.org/10.1002/nau.23172.

13. Gefen A. The role of the thermal conductivity of dressings in prevention and treatment of wounds. *Wounds Int*. 2021;12(1):18-24.

14. Kottner J, Black J, Call E, Gefen A, Santamaria N. Microclimate: a critical review in the context of pressure ulcer prevention. *Clin Biomech*. 2018;59:62-70. https://doi.org/10.1016/j.clinbiomech.2018.09.010.

15. Kayser SA, Vangilder CA, Ayello EA, Lachenbruch C. Prevalence and analysis of medical device-related pressure injuries: results from the international pressure ulcer prevalence survey. *Adv Skin Wound Care*. 2018;31(6):276-285. https://doi.org/10.1097/01.ASW.0000532475.11971.aa.

16. Carron M, Freo U, BaHammam AS, et al. Complications of non-invasive ventilation techniques: a comprehensive qualitative review of randomized trials. *Br J Anaesth*. 2013;110(6):896-914. https://doi.org/10.1093/bja/aet070.

17. Bishopp A, Oakes A, Antoine-Pitterson P, Chakraborty B, Comer D, Mukherjee R. The preventative effect of hydrocolloid dressings on nasal bridge pressure ulceration in acute non-invasive ventilation. *Ulster Med J*. 2019;88(1):17-20.

18. Munckton K, Ho KM, Dobb GJ, Das-Gupta M, Webb SA. The pressure effects of facemasks during noninvasive ventilation: a volunteer study. *Anaesthesia*. 2007;62(11):1126-1131. https://doi.org/10.1111/j.1365-2044.2007.05190.x.

19. Alqahtani JS, Worsley P, Voegeli D. Effect of humidified noninvasive ventilation on the development of facial skin breakdown. *Respir Care*. 2018;63(9):1102-1110. https://doi.org/10.4187/respcare.06087.

20. Hogeling M, Fardin SR, Frieden IJ, Wargon O. Forehead pressure necrosis in neonates following continuous positive airway pressure. *Pediatr Dermatol*. 2012;29(1):45-48. https://doi.org/10.1111/j.1525-1470.2011.01537.x.

21. Nist MD, Rodgers EA, Ruth BM, et al. Skin rounds: a quality improvement approach to enhance skin care in the neonatal intensive care unit. *Adv Neonatal Care*. 2016;16(suppl 5S):S33-S41. https://doi.org/10.1097/ANC.0000000000000337.

22. Ahmad Z, Venus M, Kisku W, Rayatt SS. A case series of skin necrosis following use of non invasive ventilation pressure masks. *Int Wound J*. 2013;10:87-90.

23. Rathore FA, Ahmad F, Zahoor MUU. Case report of a pressure ulcer occurring over the nasal bridge due to a non-invasive ventilation facial mask. *Cureus*. 2016;8(10):e813. https://doi.org/10.7759/cureus.813.

24. Haymes E. The effects of continuous positive airway pressure (CPAP) on nasal skin breakdown. *J Neonatal Nurs*. 2020;26(1):37-42. https://doi.org/10.1016/j.jnn.2019.09.007.

25. Kuo CY, Wootten CT, Tylor DA, Werkhaven JA, Huffman KF, Goudy SL. Prevention of pressure ulcers after pediatric tracheotomy using a Mepilex Ag dressing. *Laryngoscope*. 2013;123(12):3201-3205. https://doi.org/10.1002/lary.24094.

26. Forni C, Loro L, Tremosini M, et al. Use of polyurethane foam inside plaster casts to prevent the onset of heel sores in the population at risk. A controlled clinical study. *J Clin Nurs*. 2011;20(5–6):675-680. https://doi.org/10.1111/j.1365-2702.2010.03458.x.

27. Weng MH. The effect of protective treatment in reducing pressure ulcers for non-invasive ventilation patients. *Intensive Crit Care Nurs*. 2008;24(5):295-299. https://doi.org/10.1016/j.iccn.2007.11.005.

28. Linder-Ganz E, Engelberg S, Scheinowitz M, Gefen A. Pressure-time cell death threshold for albino rat skeletal muscles as related to pressure sore biomechanics. *J Biomech*. 2006;39(14):2725-2732. https://doi.org/10.1016/j.jbiomech.2005.08.010.

29. Gefen A, Alves P, Creehan S, Call E, Santamaria N. Computer modeling of prophylactic dressings: an indispensable guide for healthcare professionals. *Adv Skin Wound Care*. 2019;32(7S suppl 1):S4-S13. https://doi.org/10.1097/01.ASW.0000558695.68304.41.

30. Gefen A, Santamaria N, Creehan S, Black J. Patient safety may be compromised if study conclusions are generalized to products that make similar claims but have no equivalent research evidence. *J Patient Saf Risk Manag*. 2019;24(1):37-45. https://doi.org/10.1177/2516043518809235.

31. Schwartz D, Gefen A. An integrated experimental-computational study of the microclimate under dressings applied to intact weight-bearing skin. *Int Wound J*. 2020;17(3):562-577. https://doi.org/10.1111/iwj.13309.

32. Gefen A, Krämer M, Brehm M, Burckardt S. The biomechanical efficacy of a dressing with a soft cellulose fluff core in prophylactic use. *Int Wound J*. 2020;17(6):1968-1985. https://doi.org/10.1111/iwj.13489.

33. Gefen A. Pressure ulcer prevention dressing design and biomechanical efficacy. *J Wound Care*. 2020;29:S6-S15. https://doi.org/10.12968/jowc.2020.29.Sup12.S6.

34. Sopher R, Gefen A. Effects of skin wrinkles, age and wetness on mechanical loads in the stratum corneum as related to skin lesions. *Med Biol Eng Comput*. 2011;49(1):97-105. https://doi.org/10.1007/s11517-010-0673-3.

35. Montain SJ, Cheuvront SN, Lukaski HC. Sweat mineral-element responses during 7 h of exercise-heat stress. *Int J Sport Nutr Exerc Metab*. 2007;17(6):574-582. https://doi.org/10.1123/ijsnem.17.6.574.

36. Dąbrowska AK, Rotaru GM, Derler S, et al. Materials used to simulate physical properties of human skin. *Skin Res Technol*. 2016;22(1):3-14. https://doi.org/10.1111/srt.12235.

37. Cui C-Y, Schlessinger D. Eccrine sweat gland development and sweat secretion. *Exp Dermatol*. 2015;24(9):644-650. https://doi.org/10.1111/exd.12773.

38. Villiger M, Stoop R, Vetsch T, et al. Evaluation and review of body fluids saliva, sweat and tear compared to biochemical hydration assessment markers within blood and urine. *Eur J Clin Nutr*. 2018;72(1):69-76. https://doi.org/10.1038/ejcn.2017.136.

39. Alviset S, Riller Q, Aboab J, et al. Continuous Positive Airway Pressure (CPAP) face-mask ventilation is an easy and cheap option to manage a massive influx of patients presenting acute respiratory failure during the SARS-CoV-2 outbreak: a retrospective cohort study. *PLoS One*. 2020;15(10):e0240645. https://doi.org/10.1371/journal.pone.0240645.

40. Jessen C. *Temperature Regulation in Humans and Other Mammals*. 1st ed. Berlin, Germany: Springer-Verlag Berlin Heidelberg; 2000.

41. ASTM D575 - 91(2018) Standard Test Methods for Rubber Properties in Compression. https://www.astm.org/Standards/D575.htm. Accessed February 25, 2021.

42. Ranamukhaarachchi SA, Lehnert S, Ranamukhaarachchi SL, et al. A micromechanical comparison of human and porcine skin before and after preservation by freezing for medical device development. *Sci Rep*. 2016;6:1-9. https://doi.org/10.1038/srep32074.

43. Debeer S, le Luduec JB, Kaiserlian D, et al. Comparative histology and immunohistochemistry of porcine versus human skin. *Eur J Dermatol*. 2013;23(4):456-466. https://doi.org/10.1684/ejd.2013.2060.

44. Schwartz D, Magen YK, Levy A, Gefen A. Effects of humidity on skin friction against medical textiles as related to prevention of pressure injuries. *Int Wound J*. 2018;15(6):866-874. https://doi.org/10.1111/iwj.12937.

45. Bison P, Grinzato E. IR thermography applied to the assessment of thermal conductivity of building materials. Paper presented at: Thermosense XXXII, 2010, 7661:76610G. doi: https://doi.org/10.1117/12.849662

46. Thermal Conductivity of Metals, Metallic Elements and Alloys. https://www.engineeringtoolbox.com/thermal-conductivity-metals-d_858.html. Accessed March 12, 2021.

47. Levy A, Kopplin K, Gefen A. Device-related pressure ulcers from a biomechanical perspective. *J Tissue Viability*. 2017;26(1):57-68. https://doi.org/10.1016/j.jtv.2016.02.002.

48. Amrani G, Gefen A. Which endotracheal tube location minimises the device-related pressure ulcer risk: the Centre or a corner of the mouth? *Int Wound J*. 2020;17(2):268-276. https://doi.org/10.1111/iwj.13267.

49. Sullivan CF, Issa FG, Berthon Jones M. Home treatment of obstructive sleep apnoea with continuous positive airway pressure applied through a nose-mask. *Bull Eur Physiopathol Respir*. 1984;20(1):49-54.

50. Cai JY, Zha ML, Chen HL. Use of a hydrocolloid dressing in the prevention of device-related pressure ulcers during noninvasive ventilation: a meta-analysis of randomized controlled trials. *Wound Manag Prev*. 2019;65(2):30-38. https://doi.org/10.25270/wmp.2019.2.3038.

51. Gasparino RC, Lima MHM, de Souza Oliveira-Kumakura AR, da Silva VA, de Jesus Meszaros M, Antunes IR. Prophylactic dressings in the prevention of pressure ulcer related to the use of personal protective equipment by health professionals facing the COVID-19 pandemic: a randomized clinical trial. *Wound Repair Regen*. 2021;29(1):183-188. https://doi.org/10.1111/wrr.12877.

52. Menzella F, Barbieri C, Fontana M, et al. Effectiveness of non-invasive ventilation in COVID-19 related-acute respiratory distress syndrome. *Clin Respir J*. 2021. https://doi.org/10.1111/crj.13361.

53. Worsley PR, Prudden G, Gower G, Bader DL. Investigating the effects of strap tension during non-invasive ventilation mask application: a combined biomechanical and biomarker approach. *Med Devices*. 2016;9:409-417.

54. Zheng Y, Mak AFT. Effective elastic properties for lower limb soft tissues from manual indentation experiment. *IEEE Trans Rehabil Eng*. 1999;7(3):257-267. https://doi.org/10.1109/86.788463.

55. Kalra A, Lowe A. Mechanical behaviour of skin: a review. *J Mater Sci Eng*. 2016;5(4):1-7. https://doi.org/10.4172/2169-0022.1000254.

56. Flynn C, Taberner AJ, Nielsen PMF, Fels S. Simulating the three-dimensional deformation of in vivo facial skin. *J Mech Behav Biomed Mater*. 2013;28:484-494. https://doi.org/10.1016/j.jmbbm.2013.03.004.

57. Dai A, Wang S, Zhou L, Wei H, Wang Z, He W. In vivo mechanical characterization of human facial skin combining curved surface imaging and indentation techniques. *Skin Res Technol*. 2019;25(2):142-149.

58. Meier YA, Zhang K, Spencer ND, Simic R. Linking friction and surface properties of hydrogels molded against materials of different surface energies. *Langmuir*. 2019;35(48):158.

59. Craciunescu OI, Howle LE, Clegg ST. Experimental evaluation of the thermal properties of two tissue equivalent phantom materials. *Int J Hyperthermia*. 1999;15(6):509-518. https://doi.org/10.1080/026567399285503.

60. Tang N, Peng Z, Guo R, et al. Thermal transport in soft PAAm hydrogels. *Polymers*. 2017;9(12):688.

61. Lemmon EW, Huber ML, McLinden MO. NIST Standard Reference Database 23: Reference Fluid Thermodynamic and Transport Properties-REFPROP, Version 9.1, Natl. Inst. Stand. Technol., Gaithersbu, (Natl Std. Ref. Data Series (NIST NSRDS)); 2010.

62. Sengers J, Watson J. Improved international formulations for the viscosity and thermal conductivity of water substance. *Am Chem Soc Am Inst Phys Natl Bur Stand*. 1986;15(4):1291-1314.

63. Webb RC, Pielak RM, Bastien P, et al. Thermal transport characteristics of human skin measured in vivo using ultrathin conformal arrays of thermal sensors and actuators. *PLoS One*. 2015;10(2):e011. https://doi.org/10.1371/journal.pone.0118131.

64. Krishnan S, Shi Y, Webb RC, et al. Multimodal epidermal devices for hydration monitoring. *Microsyst Nanoeng*. 2017;3:17014.

65. Crawford KE, Ma Y, Krishnan S, et al. Advanced approaches for quantitative characterization of thermal transport properties in soft materials using thin, conformable resistive sensors. *Extreme Mech Lett*. 2018;22:27-35. https://doi.org/10.1016/j.eml.2018.04.002.

66. Tian LM, Li YH, Webb RC, et al. Flexible and stretchable 3 omega sensors for thermal characterization of human skin. *Adv Funct Mater*. 2017;27:1701282.

67. Gun'ko VM, Savina IN, Mikhalovsky SV. Properties of water bound in hydrogels. *Gels*. 2017;3(4):37.

68. Tran VT, Mredha TI, Jeon I. High-water-content hydrogels exhibiting superior stiffness, strength, and toughness. *Extrem Mech Lett*. 2020;37:100691.

69. Johnsen GK, Martinsen OG, Grimnes S. Estimation of in vivo water content of the stratum corneum from electrical measurements. *Open Biomed Eng J*. 2009;3:8-12.

70. Logger JGM, Münchhoff CU, Olydam JI, Peppelman M, van Erp PEJ. Anatomical site variation of water content in human skin measured by the Epsilon: a pilot study. *Skin Res Technol*. 2019;25(3):333.

71. Egawa M, Yanai M, Maruyama N, Fukaya Y, Hirao T. Visualization of water distribution in the facial epidermal layers of skin using high-sensitivity near-infrared (NIR) imaging. *Appl Spectrosc*. 2015;69(4):481-487.

72. Pethig R, Kell DB. The passive electrical properties of biological systems: their significance in physiology, biophysics and biotechnology. *Phys Med Biol*. 1987;32 (8):933.

73. Zeevi T, Levy A, Brauner N, Gefen A. Effects of ambient conditions on the risk of pressure injuries in bedridden patients-multi-physics modelling of microclimate. *Int Wound J*. 2018;15 (3):402-416.